Acta Cryst. (1976). A32, 869

The Thermal Neutron Scattering by Single Crystals. Reflectivity and Secondary Extinction

BY S. G. BOGDANOV AND A. Z. MENSHIKOV

620066, *Institute of Metal Physics of the Academy of Sciences of the USSR, Sverdlovsk, GSP*-170, *USSR*

(*Received* 20 *August* 1975; *accepted* 15 *March* 1976)

General equations for integral and peak reflectivity and also the secondary extinction coefficient of crystals have been derived in unified form for a plate, cylinder and sphere in reflexion and transmission. The numerical calculations of these formulae have been carried out. The dependence on both the scattering and absorption coefficients, the mosaic spread parameter, the crystal size, and beam collimation are discussed separately with respect to the secondary extinction and the scattering geometry. Experimental verification conditions for the theoretical calculations are considered too.

Introduction

The wide use of single crystals of different materials in experimental neutron diffraction techniques necessitates the theoretical research of reflectivity. But in single-crystal structural investigations the secondary extinction effect is of great importance and is calculated theoretically too. As is known from the kinematic theory, the reflectivity and the secondary extinction coefficient are mutually related.

In the application to X-rays the above-mentioned problems have been considered by Zachariasen (1945) and James (1950). Detailed research of the intensity of thermal neutrons scattered by a mosaic crystal has been carried out by Bacon & Lowde (1948). They have derived the equation for the integrated reflectivity (R^θ) of a plane parallel plate crystal for an ideal parallel monochromatic neutron beam. The calculation of the integrated reflectivity has been carried out in the rotating-crystal method, which is equivalent to the R^θ for a fixed crystal onto which a neutron beam with infinite divergence impinges.

The calculation of the finite divergence of a neutron beam has been carried out by Kunitomi, Sakamoto, Hamaguchi & Betsugaku (1964) in reflexion and by Dietrich & Als-Nielsen (1965) in transmission. The luminosity and resolution of the neutron spectrometer, taking into account the neutron beam collimation, have been considered by Sailor, Foote, Landon & Wood (1956), Abov (1960), Caglioti & Ricci (1962) and in more detail by Popovici & Gelberg (1966). Hamilton (1963) and Nosik (1966) have carried out the calculation of the secondary extinction coefficient (E_s) for cylindrical and spherical crystals respectively.

However in the above-mentioned papers in order to simplify the problem some approximations were taken into consideration, *i.e.* either the absorption or the neutron beam divergence was not taken into account. The peak reflectivity (R_p) was not considered in general formulation in any of the papers.

The purpose of the present study is to derive general equations (where ones are absent) for R^θ, R_p and E_s for widely distributed crystal shapes, plate, cylinder and sphere, and to carry out the comparative numerical analysis by electronic computer. As a utilitarian task it was of interest to compile R^θ, R_p and E_s tables convenient for wide practical use. The question of their experimental measurement by existing spectrometers is also discussed.

General definitions and formulae

We define the reflectivity as the ratio between the scattered neutron current (P_1) and the incoming neutron current (P_0). In general it is a function of the reflexion angle (θ) and the deviation (Δ) of the mosaic block from the average orientation in accordance with the exact Wolf–Bragg condition:

$$P(\theta,\Delta)=\frac{P_1}{P_0}.$$

P_1 is determined from the differential-equation system which describes parallel neutron beam propagation in an ideally imperfect crystal. These equations have been given in their most general form by Moon & Shull (1964).

As we are considerably interested in the reflectivity of a crystal as a neutron monochromator we will consider the system consisting of a fixed crystal and two collimators placed in front and behind the crystal with divergences α_1 and α_2 respectively. Hence, we first write the integrated reflectivity for monochromatic neutrons as

$$R^\theta=\int_{-\infty}^{\infty} n_1(\varphi_1)P(\theta,\Delta)n_2(\varphi_2)\mathrm{d}\Delta, \qquad (1)$$

where the mosaic distribution function [$W(\Delta)$] and the collimator acceptance function [$n_i(\varphi_i)$] are approximated by Gaussians:

$$W(\Delta)=\frac{1}{\sqrt{2\pi\eta}}\exp\left(-\frac{\Delta^2}{2\eta^2}\right), \qquad (2)$$

$$n_i(\varphi_i)=\exp\left(-\frac{\varphi_i^2}{\alpha_i^2}\right), \quad i=1,2. \qquad (3)$$

Here η, the 'mosaic spread', is the standard deviation of the distribution, φ_i is the angle between the trajectory of the neutrons and the central path through the collimator in horizontal projection, $\alpha_i/\sqrt{2}$ is the standard deviation related functionally to the collimator width s_i and length l_i by:

$$\alpha_i = \frac{s_i}{l_i 2\sqrt{\ln 2}} . \tag{4}$$

The peak reflectivity will be expressed as the ratio between the scattered and the incoming neutron currents if the crystal is set in the exact Wolf–Bragg position ($\Delta=0$):

$$R_p = P(\theta,0). \tag{5}$$

Consequently, if the integrated reflectivity for monochromatic neutrons is considered as the area under the reflexion curve, the peak reflectivity is the maximum ordinate of this curve. It is clear that R_p ($\lambda=$const.) does not depend on the incoming neutron beam divergence.

The integrated reflectivity for a white divergent beam is defined as the relation between the current of the scattered neutrons passed through the second collimator and the current of incoming neutrons passed through the first and the second collimators set together. Taking into account the following relations [see for example, Dietrich & Als-Nielsen (1965)]

$$\left.\begin{aligned} \varphi_1 &= \theta - \theta_B - \Delta \\ \varphi_2 &= \theta - \theta_B + \Delta \end{aligned}\right\}, \tag{6}$$

where θ_B is the Wolf–Bragg angle, θ is the reflexion angle of an individual beam, we may write in this case, according to Popovici, Gheorghiu & Gelberg (1968),

$$R^\theta = \frac{1}{N}\int_{-\infty}^{\infty}\int_{-\infty}^{\infty}\int_{-\infty}^{\infty} n_1(\varphi_1)P(\theta,\Delta)n_2(\varphi_2) \times \delta(\varphi_1-\varphi_2+2\Delta)\mathrm{d}\varphi_1\mathrm{d}\varphi_2\mathrm{d}\Delta, \tag{7}$$

where

$$N = \int_{-\infty}^{\infty}\int_{-\infty}^{\infty} n_1(\varphi_1)n_2(\varphi_2)\delta(\varphi_1-\varphi_2)\mathrm{d}\varphi_1\mathrm{d}\varphi_2. \tag{8}$$

Analogously we may write for $R_p(\lambda\neq\text{const.})$

$$R_p = \frac{1}{N_1}\int_{-\infty}^{\infty}\int_{-\infty}^{\infty}\int_{-\infty}^{\infty} n_1(\varphi_1)P(\theta,\Delta)n_2(\varphi_2) \times \delta(\varphi_1-\varphi_2+2\Delta)\delta(\varphi_2)\mathrm{d}\varphi_1\mathrm{d}\varphi_2\mathrm{d}\Delta, \tag{9}$$

where

$$N_1 = \int_{-\infty}^{\infty} n_1(\varphi_1)\mathrm{d}\varphi_1. \tag{10}$$

For the case $\lambda\neq$const. the integrated reflectivity may be represented as the area under the reflexion curve *versus* the angle between the trajectory of the neutrons and the central path through the second collimator; the peak reflectivity is the value proportional to the maximum ordinate at $\varphi_2=0$.

The equations (1) and (7) may be written in the common form

$$R^\theta = \int_{-\infty}^{\infty} P(\theta,\Delta)\exp\left(-\frac{2\Delta^2}{\alpha_e^2}\right)\mathrm{d}\Delta, \tag{11}$$

where

$$\alpha_e = \begin{cases} \dfrac{\sqrt{2}\alpha_1\alpha_2}{\sqrt{\alpha_1^2+\alpha_2^2}}, & \text{if } \lambda=\text{const.} \\ \sqrt{\dfrac{\alpha_1^2+\alpha_2^2}{2}}, & \text{if } \lambda\neq\text{const.} \end{cases} \tag{12}$$

In addition, for a white neutron beam using (7) and (9) we obtain the following relation

$$R_p = \frac{1}{\alpha_1\sqrt{\pi}} R^\theta \tag{13}$$

if we put $\alpha_e=\alpha_1/\sqrt{2}$. When $\alpha_1\to 0$ $R_p(\lambda\neq\text{const.})\to \frac{1}{2}R_p(\lambda=\text{const.})$, and when $\alpha_1=\alpha_2=\alpha$ $R^\theta(\lambda\neq\text{const.})=R^\theta(\lambda=\text{const.})$. Thus the peak reflectivity for the white divergent neutron beam is always less than R_p for the monochromatic neutron beam; but integrated reflectivity values are equal for symmetrical collimation ($\alpha_1=\alpha_2$) in both cases. This reveals the significant curve widening of reflected non-monochromatic neutrons compared with monochromatic neutrons.

In order to describe the secondary extinction effect quantitatively the secondary extinction coefficient is usually introduced as the ratio between the integrated reflectivity R^θ calculated with the secondary extinction correction and integrated reflectivity R^θ_{id} obtained without the extinction correction but taking into account the other factors: absorption, crystal geometry, incident and scattered flux divergences:

$$E_s = \frac{R^\theta}{R^\theta_{\mathrm{id}}} . \tag{14}$$

Therefore, the calculation of the secondary extinction coefficient is closely related to the calculation of reflectivities.

The equations describing integrated and peak reflectivities for differently shaped single crystals for symmetrical reflexion and transmission are presented in general form in Table 1. All the formulae are obtained in the present paper (see the Appendix) except equations (15) and (17) which were first derived by Kunitomi *et al.* (1964) and Dietrich & Als-Nielsen (1965) respectively. The distinctive feature of equations (15) to (18) is their validity for any neutron scattering angle. For the spherical and cylindrical single crystals the analytical equations for R^θ and R_p can be obtained only in two boundary cases: $2\theta=0°$ (forward scattering) and $2\theta=180°$ (back scattering).

In Table 1 formulae are presented for the peak reflectivity of monochromatic neutrons. For non-monochromatic neutrons R_p values may be obtained taking into account equation (13).

Corresponding equations for secondary extinction are presented in Table 2. Formula (28) was first derived by Dietrich & Als-Nielsen (1965) and formulae (29) and (30), without accounting for the divergence effect, by Hamilton (1957).

Discussion

(*a*) *The calculation*

Reflectivities and secondary extinction coefficients of plate, cylinder, and sphere-shaped single crystals were calculated in reflexion and transmission by numerical methods using the computer BESM-6 according to the formulae given in Tables 1 and 2 with the following fixed variables:

$\frac{Q}{\mu}$ = 0·001; 0·005; 0·01; 0·05; 0·1; 1·0; 10·0;

C = 0·01; 0·1; 0·5; 1·0; 2·0; 3·0; 4·0; 6·0; 10·0;

η = 4′; 8′; 16′; 32′; 64′;

α_e = 6′; 12′; 24′; 48′; 96′;

(The quantities Q/μ and C are defined in the footnote to Table 1).

Let us consider the principal regularities which follow from the present calculations. In Fig. 1 the dependence of R^θ on the logarithm of the mosaic spread for different Q/μ values is illustrated. As one can see, in contrast to the dotted Bacon–Lowde curves the R^θ curves, with due regard for the neu-

Table 1. *The analytical formulae for the integrated and peak reflectivities*

Plate

In reflexion

$$R^\theta = \eta \int_{-\infty}^{\infty} \frac{A \exp(-Bx^2/2)\mathrm{d}x}{(1+A\exp -x^2/2)+(1+2A\exp -x^2/2)^{1/2}\coth[C(1+2A\exp -x^2/2)^{1/2}]} \tag{15}$$

$$R_p = \frac{A}{1+A+(1+2A)^{1/2}\coth[C(1+2A)^{1/2}]} \tag{16}$$

In transmission

$$R^\theta = \eta \sqrt{\frac{\pi}{2}} \exp(-C) \sum_{j=1}^{\infty} \frac{(-1)^{j+1}}{j!} \frac{(2AC)^j}{\sqrt{j-1+B}} \tag{17}$$

$$R_p = \tfrac{1}{2}\exp(-C)[1-\exp(-2AC)] \tag{18}$$

Cylinder

In reflexion, $2\theta = 180°$

$$R^\theta = \eta \int_{-\infty}^{\infty}\int_0^{\pi/2} \frac{A\exp(-Bx^2/2)\cos\varphi \mathrm{d}x\mathrm{d}\varphi}{(1+A\exp -x^2/2)+(1+2A\exp -x^2/2)^{1/2}\coth[C\cos\varphi[1+2A\exp -x^2/2)^{1/2}]} \tag{19}$$

$$R_p = \int_0^{\pi/2} \frac{A\cos\varphi \mathrm{d}\varphi}{1+A+(1+2A)^{1/2}\coth[C\cos\varphi(1+2A)^{1/2}]} \tag{20}$$

In transmission, $2\theta = 0°$

$$R^\theta = \eta \sqrt{\frac{\pi}{2}} \sum_{j=1}^{\infty} \frac{(-1)^{j+1}}{j!} \frac{(2AC)^j}{\sqrt{j-1+B}} \int_0^{\pi/2} \exp(-C\cos\varphi)(\cos\varphi)^{j+1}\mathrm{d}\varphi \tag{21}$$

$$R_p = \tfrac{1}{2}\int_0^{\pi/2} \exp[-C\cos\varphi][1-\exp(-2AC\cos\varphi)]\cos\varphi \mathrm{d}\varphi \tag{22}$$

Sphere

In reflexion, $2\theta = 180°$

$$R^\theta = \eta \frac{4}{\pi}\int_{-\infty}^{\infty}\int_0^{\pi/2}\int_0^{\pi/2} \frac{A\exp(-Bx^2/2)\cos^2\varphi\cos\psi \mathrm{d}x\mathrm{d}\varphi\mathrm{d}\psi}{(1+A\exp -x^2/2)+(1+2A\exp -x^2/2)^{1/2}\coth[C\cos\varphi\cos\psi(1+2A\exp -x^2/2)^{1/2}]} \tag{23}$$

$$R_p = \frac{4}{\pi}\int_0^{\pi/2}\int_0^{\pi/2} \frac{A\cos^2\varphi\cos\psi \,\mathrm{d}\varphi\mathrm{d}\psi}{1+A+(1+2A)^{1/2}\coth[C\cos\varphi\cos\psi(1+2A)^{1/2}]} \tag{24}$$

In transmission, $2\theta = 0°$

$$R^\theta = \eta \frac{4}{\pi}\sqrt{\frac{\pi}{2}} \sum_{j=1}^{\infty} \frac{(-1)^{j+1}}{j!} \frac{(2AC)^j}{\sqrt{j-1+B}} \int_0^{\pi/2}\int_0^{\pi/2} \exp(-C\cos\varphi\cos\psi)(\cos\varphi)^{j+2}(\cos\psi)^{j+1}\mathrm{d}\varphi\mathrm{d}\psi \tag{25}$$

$$R_p = \frac{2}{\pi}\int_0^{\pi/2}\int_0^{\pi/2} \exp(-C\cos\varphi\cos\psi)[1-\exp(-2AC\cos\varphi\cos\psi)]\cos^2\varphi\cos\psi\mathrm{d}\varphi\mathrm{d}\psi \tag{26}$$

Notation

$$A = \frac{Q}{\mu\eta\sqrt{2\pi}}\,;\quad B = 1+\frac{4\eta^2}{\alpha_e^2}\quad C = \frac{\mu D}{\gamma}\,;\quad Q = \frac{\lambda^3F^2N_c^2}{\sin 2\theta}$$

$\gamma = \begin{cases} 1 & \text{– cylinder and sphere} \\ \sin\theta & \text{– plate in reflexion} \\ \cos\theta & \text{– plate in transmission} \end{cases}$

λ is the wavelength; F is the structure factor

N_c is the number of unit cells per cm^3

μ is the linear attenuation coefficient allowing for the true absorption, the incoherent scattering and the thermal diffuse scattering

D is the plate thickness (or diameter of cylinder or sphere)

Coordinate x is defined as $x = \Delta/\eta$, coordinates φ and ψ are defined in (*A*4)

tron beam divergence, have their maxima in positions determined by the effective collimation. Here the dependence of R^θ on Q/μ is shown too. In Fig. 2 the dependence of the integrated reflectivity on the neutron beam divergence is demonstrated. Analysing the present curves one can conclude the importance of optimal collimator choice in the neutron diffraction technique.

The comparison of the reflectivities of differently shaped single crystals in reflexion and transmission is shown in Fig. 3. It is seen that under otherwise identical conditions R^θ is always larger in reflexion than in transmission and decreases in the order plate–cylinder–sphere except for large C values.

The relation R_p *vs* Q/μ is illustrated in Fig. 4. As can be seen, peak reflectivity boundary values equal to $\frac{1}{2}(\lambda \neq \text{const.})$ and $1(\lambda = \text{const.})$ are reached at small divergence of the incident beam and at large Q/μ values.

Some regularities of the secondary extinction coefficient are shown in Figs. 5–8. The dependence of E_s on size and shape of the specimen and on observation geometry is demonstrated in Fig. 5. Q/μ, η and α_e values are chosen close to the real existing ones in experimental situations. In this figure the strong dependence of secondary extinction on the specimen shape and the observation geometry is shown. It is important to note that the secondary extinction effect is appreciable at $C=0{\cdot}1$. In Fig. 6 the secondary extinction coefficient dependence on the mosaic spread for a plate-shaped crystal in symmetrical re-

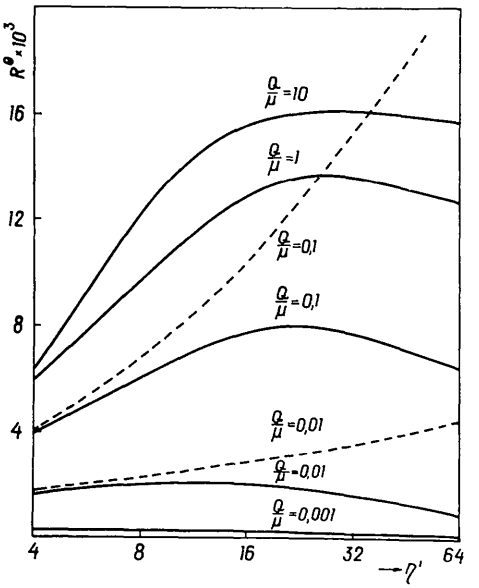

Fig. 1. Integrated reflectivity *versus* the crystal mosaic spread for a plate crystal at different Q/μ values in reflexion ($C=0{\cdot}5$; $\alpha_e=24'$); the dotted lines are the Bacon–Lowde curves (Bacon & Lowde, 1948).

Table 2. *The secondary extinction coefficient (E_s) for single crystals of plate, cylinder and sphere shapes in reflexion and transmission*

Plate

In reflexion

$$E_s=\frac{\sqrt{\frac{2B}{\pi}}}{(1-e^{-2C})}\int_{-\infty}^{\infty}\frac{\exp\left(-\frac{Bx^2}{2}\right)dx}{(1+A\exp-x^2/2)+(1+2A\exp-x^2/2)^{1/2}\coth\left[C(1+2A\exp-x^2/2)^{1/2}\right]} \tag{27}$$

In transmission

$$E_s=\sum_{j=1}^{\infty}\frac{(-1)^{j+1}}{j!}(2AC)^{j-1}\frac{\sqrt{B}}{\sqrt{j-1+B}} \tag{28}$$

Cylinder

In reflexion, $2\theta=180°$

$$E_s=\sqrt{\frac{2B}{\pi}}\cdot\frac{\int_{-\infty}^{\infty}\int_0^{\pi/2}\frac{\exp(-Bx^2/2)\cos\varphi\,dx\,d\varphi}{(1+A\exp-x^2/2)+(1+2A\exp-x^2/2)^{1/2}\coth\left[C\cos\varphi(1+2A\exp-x^2/2)^{1/2}\right]}}{\int_0^{\pi/2}[1-\exp(-2C\cos\varphi)]\cos\varphi\,d\varphi} \tag{29}$$

In transmission, $2\theta=0°$

$$E_s=\frac{\sum_{j=1}^{\infty}\frac{(-1)^{j+1}}{j!}(2AC)^{j-1}\frac{\sqrt{B}}{\sqrt{B+j-1}}\int_0^{\pi/2}\exp(-C\cos\varphi)(\cos\varphi)^{j+1}d\varphi}{\int_0^{\pi/2}\exp(-C\cos\varphi)\cos^2\varphi\,d\varphi} \tag{30}$$

Sphere

In reflexion, $2\theta=180°$

$$E_s=\sqrt{\frac{2B}{\pi}}\cdot\frac{\int_{-\infty}^{\infty}\int_0^{\pi/2}\int_0^{\pi/2}\frac{\exp(-Bx^2/2)\cos^2\varphi\cos\psi\,dx\,d\varphi\,d\psi}{(1+A\exp-x^2/2)+(1+2A\exp-x^2/2)^{1/2}\coth\left[C\cos\varphi\cos\psi(1+2A\exp-x^2/2)^{1/2}\right]}}{\int_0^{\pi/2}\int_0^{\pi/2}\cos^2\varphi\cos\psi[1-\exp(-2C\cos\varphi\cos\psi)]d\varphi\,d\psi} \tag{31}$$

In transmission, $2\theta=0°$

$$E_s=\frac{\sum_{j=1}^{\infty}\frac{(-1)^{j+1}}{j!}(2AC)^{j-1}\frac{\sqrt{B}}{\sqrt{j-1+B}}\int_0^{\pi/2}\int_0^{\pi/2}\exp(-C\cos\varphi\cos\psi)(\cos\varphi)^{j+2}(\cos\psi)^{j+1}d\varphi\,d\psi}{\int_0^{\pi/2}\int_0^{\pi/2}\exp(-C\cos\varphi\cos\psi)\cos^3\varphi\cos^2\psi\,d\varphi\,d\psi} \tag{32}$$

flexion at various Q/μ values is shown. It is seen that secondary extinction increases if the mosaic spread and Q/μ increase. The secondary extinction coefficient depends on the neutron beam collimation to a lesser degree (Fig. 7).

(b) The comparison with experiment

Our calculated R^θ and R_p values are related to the single-crystal spectrometer case where the scattered neutrons are detected by a fixed detector set in the reflexion position. These conditions correspond to those of using the crystal as a monochromator. Then, in order to correct theoretical formulae one can use the double-crystal spectrometer system where the first crystal is a monochromator and the second is a specimen. In this case the reflexion curve may be detected by both θ and θ–2θ scanning methods. Obviously the data obtained by these methods do not coincide; what is more, each method provides the possibility of obtaining different information about the single-crystal reflectivity. We now consider this in detail.

First of all, in order to carry out the experimental R^θ measurement by a double-crystal spectrometer method it is necessary to choose as a monochromator a single crystal as perfect as possible. Then the white divergent neutron beam scattered by such a monochromator is dispersed. If such a beam impinges on the second crystal (specimen) and the reflexion curve is detected by the θ-scan method one can derive in accordance with (7)

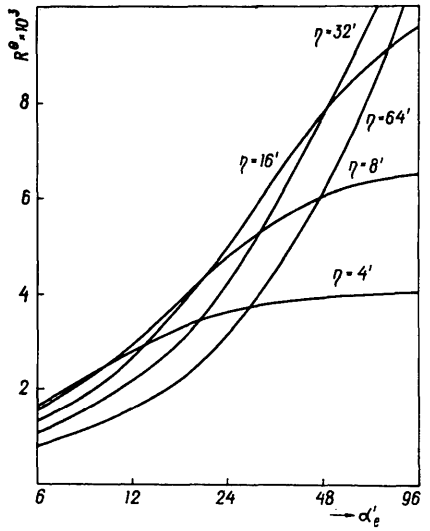

Fig. 2. Integrated reflectivity *versus* neutron beam collimation at different mosaic spreads (plate in reflexion; $Q/\mu=0{\cdot}1$, $C=0{\cdot}5$).

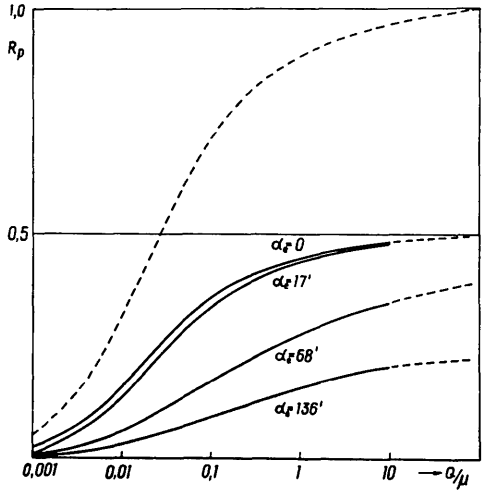

Fig. 4. Peak single-crystal reflectivity *versus* Q/μ (plate in the reflexion, $C=0{\cdot}5$, $\eta=8'$): dotted lines – $\lambda=$const., solid lines – $\lambda\neq$const.

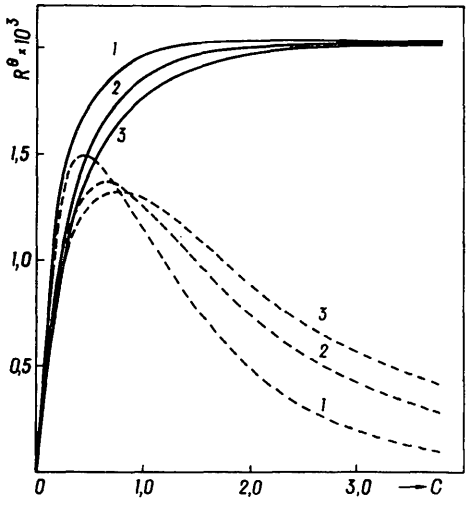

Fig. 3. Integrated single-crystal reflectivity *versus* the size for various crystal shapes ($C=\mu D/\gamma$, $Q/\mu=0{\cdot}01$, $\eta=8'$, $\alpha_e=24'$): solid lines – reflexion, dotted lines – transmission; (1) plate, (2) cylinder, (3) sphere.

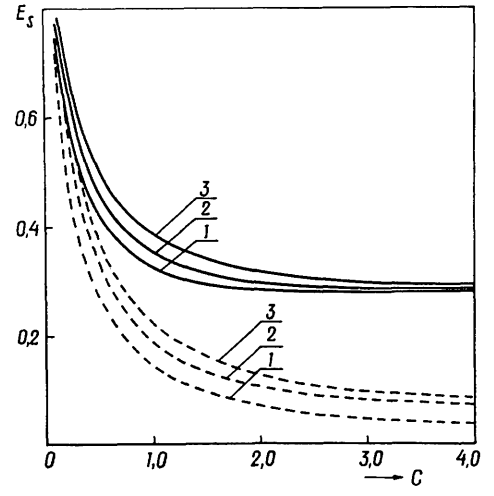

Fig. 5. Secondary extinction coefficient *versus* crystal size for various shapes ($C=\mu D/\gamma$): solid lines – reflexion; dotted lines – transmission; (1) plate, (2) cylinder, (3) sphere.

$$R^{\theta}(\varrho)=\frac{1}{N}\int_{-\infty}^{\infty}P[\theta,(a-1)\varphi_1-\varrho]\times n_1(\varphi_1)n_2[(2a-1)\varphi_1]\mathrm{d}\varphi_1, \quad (33)$$

where ϱ is the rotation angle of the crystal, $a(=\tan\theta/\tan\theta_M)$ is the dispersion parameter, θ_M is the Wolf–Bragg angle of the monochromator. At $a=1$

$$\int_{-\infty}^{\infty}R^{\theta}(\varrho)\mathrm{d}\varrho=\int_{-\infty}^{\infty}P(\theta,\varrho)\mathrm{d}\varrho \quad (34)$$

indicating the independence of the reflexion curve from the collimator divergences α_1 and α_2. Experimentally such detection conditions have been used by Riste & Otnes (1969) and Dymond & Brockhouse (1970) for the measurement of integrated and peak reflectivities in the rotating crystal method and to verify the validity of the Bacon–Lowde (1948) formulae.

If the reflexion curve is obtained by θ–2θ scanning, the integrated reflectivity *vs* crystal rotation angle ϱ may be defined as

$$R^{\theta}(\varrho)=\frac{1}{N}\int_{-\infty}^{\infty}P[\theta,(a-1)\varphi_1-\varrho]\times n_1(\varphi_1)n_2[(2a-1)\varphi_1+2\varrho]\mathrm{d}\varphi_1. \quad (35)$$

At $a=1$ the area under the reflexion curve will describe the white divergent neutron beam reflectivity with the restricted collimation of the first and second collimators:

$$\int R^{\theta}(\varrho)\mathrm{d}\varrho=\int_{-\infty}^{\infty}P(\theta,\varrho)\exp\left(-\frac{4\varrho^2}{\alpha_1^2+\alpha_2^2}\right)\mathrm{d}\varrho. \quad (36)$$

Consequently by the θ–2θ scanning method the integrated reflectivity corresponding to the real conditions of the monochromator crystal is measured, *i.e.* by this method one can verify the validity of the formulae for the integrated reflectivity.

There are literature references on the experimental verification of the formulae for the integrated and peak reflectivities of the monochromatic, parallel neutron beam, *e.g.* Riste & Otnes (1969), Dymond & Brockhouse (1970), Dorner (1971). There are few papers which have been devoted to the verification of the integrated reflectivity formulae presented in Table 1. In Fig. 8, some experimental results (after Popovici, Gheorghiu & Gelberg, 1968) in comparison with our theoretical curves are shown. As the experimental determination of R^{θ} was relative, these points were scaled to fit the first to the theoretical curve. As one can see, the behaviour of the experimental and theoretical curves is very similar and the fit between them is quite good. It should be noted that our calculated curves, which are represented in this figure, and the theoretical curves of Popovici *et al.* (1968) fit each other with great exactness.

It is of natural interest to compare the secondary extinction coefficient values which have been obtained here with the calculations by Zachariasen's (1967) theory. He considered the general X-ray scattering by crystals for which the mosaic width β may be comparable to or less than the diffraction line width ε_1 of an ideal, small-size, perfect crystal. He has pointed out that if $\beta\gg\varepsilon_1$ then the secondary extinction coefficient depends on the crystal mosaic parameter only (type I crystals); and if $\beta\ll\varepsilon_1$ it depends on mosaic block size only (type II crystals). If the crystal is neither type I nor type II both the mosaic spread and the crystal mosaic block size influence the secondary extinction. The applicability of Zachariasen's theory to neutron diffraction was discussed by Cooper & Rouse (1970)

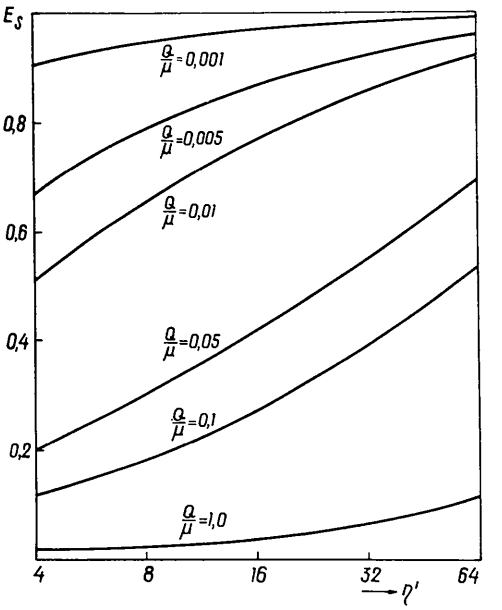

Fig. 6. Secondary extinction coefficient *versus* single-crystal mosaic spread at different Q/μ values (plate in reflexion; $C=0{\cdot}5$; $\alpha_e=24'$).

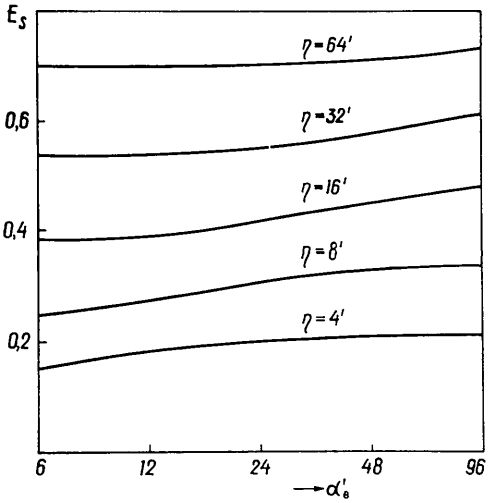

Fig. 7. Secondary extinction coefficient *versus* neutron beam divergence at different crystal mosaic spreads in reflexion ($Q/\mu=0{\cdot}05$; $C=0{\cdot}5$).

and Cooper, Rouse & Fuess (1973). In order to explain the experimental neutron data they slightly modified the Zachariasen equation for the secondary extinction coefficient and carried out the calculation of E_s for a sphere-shaped single crystal of ZnS which is, according to their data, a type I crystal with the mosaic parameter $g \equiv 1/(2\sqrt{\pi\eta}) = 1390 \pm 360$. For the comparison we have calculated E_s for such a specimen too. The data are given in Table 3. There is some disagreement between our calculation and the data of Cooper *et al.* (1973). Such disagreement may be due to two factors: (1) the g parameter cannot be determined quite exactly because of the primary extinction, which is present even in the best agreement between theory and experiment; (2) it is to be expected that at $\eta < 1'$ the formulae in Table 2 are not quite valid because of the inapplicability of the kinematic approximation.

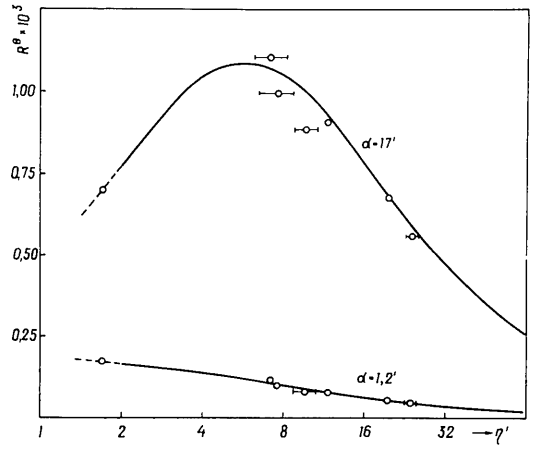

Fig. 8. The comparison between theoretical and experimental reflectivities of Pb (111) in transmission *versus* crystal mosaic spread ($t = 0{\cdot}9$ cm). Experimental points are quoted from the paper by Popovici, Gheorghiu & Gelberg (1968).

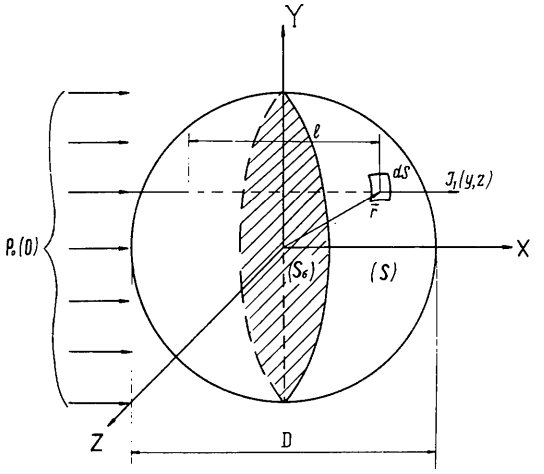

Fig. 9. Geometry of neutron scattering by a spherical sample crystal with diameter D in forward scattering ($2\theta = 0°$). [The individual beam path in the crystal is defined as $l = 2(D^2/4 - y^2 - z^2)^{1/2}$.]

Table 3. *The comparison of secondary extinction coefficient values (E_s) calculated by the formula* (32) *of Table* 2 *with the data of Cooper, Rouse & Fuess* (1973) [E_s(CRF)] *for the* ZnS *spherical single crystal of diameter* $D = 0{\cdot}22$ cm, $\lambda = 0{\cdot}873$ Å, $\eta = 0{\cdot}7'$

h k l	E_s	E_s(CRF)	h k l	E_s	E_s(CRF)
0 2 2	0·984	0·878	1 1 1	0·984	0·883
4 0 0	0·986	0·916	3 1 1	0·987	0·940
4 2 2	0·987	0·936	1 3 3	0·988	0·957
0 4 4	0·988	0·948	5 1 1	0·988	0·967
4 4 4	0·988	0·963	5 3 3	0·989	0·977
8 0 0	0·989	0·972	7 1 1	0·989	0·980
8 2 2	0·989	0·975	1 5 5	0·989	0·981
4 6 6	0·989	0·980	3 5 5	0·989	0·983
8 4 4	0·989	0·982	7 3 3	0·989	0·985
2 0 0	0·989	0·978	5 5 5	0·989	0·987
2 2 2	0·989	0·988	9 1 1	0·989	0·988
2 4 4	0·990	0·995	1 7 7	0·989	0·990
6 2 2	0·990	0·996	7 5 5	0·989	0·990
6 4 4	0·990	0·998	3 7 7	0·990	0·991
2 6 6	0·990	0·998	11 1 1	0·990	0·992
10 0 0	0·990	0·999	5 7 7	0·990	0·992
10 2 2	0·990	0·999			

The authors wish to acknowledge N. N. Lebedeva and Yu. M. Plishkin for the computer calculations and to thank Professor S. K. Sidorov for his interest in the work.

APPENDIX

We now derive the formulae presented in Tables 1 and 2. As an example (Fig. 9) we shall consider most general variant of neutron scattering by spherical samples with diameter D in forward scattering ($2\theta = 0°$). The current of scattered neutrons P_1 may be written as follows

$$P_1 = \int_{(S)} \mathrm{d}P_1 \qquad (A1)$$

where $\mathrm{d}P_1$ is the current of neutrons scattered by an infinitesimal square $\mathrm{d}S$ of the sample surface in the vicinity of a point $r[(D^2/4 - y^2 - z^2)^{1/2}, y, z]$; the integration is made over the hemisphere S which is described by the equation

$$x^2 + y^2 + z^2 = \frac{D^2}{4}, \quad x > 0 .$$

The axis X coincides with the incident beam direction.

We can express the infinitesimal current $\mathrm{d}P_1$, *via* scattered neutron intensity $I_1(y,z)$ in a point r as:

$$\mathrm{d}P_1 = I_1(y,z)\mathrm{d}\sigma \qquad (A2)$$

where $\mathrm{d}\sigma$ is the projection of the infinitesimal square $\mathrm{d}S$ on the YOZ plane. Taking into account the obvious equation

$$\int_{(S)} I_1(y,z)\mathrm{d}S = \int_{(S_\sigma)} I_1(y,z)\mathrm{d}\sigma \equiv \int_{(S_\sigma)} \int I_1(y,z)\mathrm{d}y\mathrm{d}z , \qquad (A3)$$

where S_σ is the projection of square S on the YOZ plane, and introducing the changes of variable

$$\left.\begin{aligned} z &= \frac{D}{2}\sin\varphi \\ y &= \frac{D}{2}\cos\varphi\sin\varphi \end{aligned}\right\} \qquad (A4)$$

we obtain

$$P_1 = \int_{-D/2}^{D/2} \mathrm{d}z \int_{-\sqrt{D^2/4-z^2}}^{\sqrt{D^2/4-z^2}} \mathrm{d}y I_1(y,z)$$
$$= D^2 \int_0^{\pi/2}\int_0^{\pi/2} I_1(\varphi,\psi)\cos^2\varphi\cos\psi\,\mathrm{d}\varphi\mathrm{d}\psi. \qquad (A5)$$

Considering $I_1(\varphi,\psi)$ as the scattering intensity from the plate-shaped sample of thickness $2(D^2/4-y^2-z^2)^{1/2} = D\cos\varphi\cos\psi$, one can derive analytical expressions for reflectivities and secondary extinction coefficients. Thus for $I_1(\varphi,\psi)$ we have

$$I_1(\varphi,\psi) = \tfrac{1}{2}I_0(0)\exp(-\mu D\cos\varphi\cos\psi) \times[1-\exp(-2rD\cos\varphi\cos\psi)]$$

where

$$r \equiv r(\Delta) = \frac{Q}{\sqrt{2\pi}\eta}\exp\left(-\frac{\Delta^2}{2\eta^2}\right).$$

Then taking into account $I_0(0)\pi D^2/4 = P_0(0)$ we obtain the reflectivity of a spherical single crystal

$$P(\theta,\Delta) \equiv \frac{P_1}{P_0(0)} = \frac{2}{\pi}\int_0^{\pi/2}\int_0^{\pi/2}\exp(-\mu D\cos\varphi\cos\psi) \times[1-\exp(-2rD\cos\varphi\cos\psi)]\cos^2\varphi\cos\psi\,\mathrm{d}\varphi\mathrm{d}\psi. \qquad (A6)$$

We now write with respect to (11) the integrated reflectivity taking into account the neutron beam divergence

$$R^\theta = \frac{2}{\pi}\int_0^{\pi/2}\int_0^{\pi/2}\mathrm{d}\varphi\mathrm{d}\psi\cos^2\varphi\cos\psi \times\exp(-\mu D\cos\varphi\cos\psi)\int_{-\infty}^{\infty}\mathrm{d}\Delta\exp\left(-\frac{2\Delta^2}{\alpha_e^2}\right) \times\left[1-\exp\left\{\left[-\frac{2QD\cos\varphi\cos\psi}{\sqrt{2\pi}\eta}\exp\left(-\frac{\Delta^2}{2\eta^2}\right)\right]\right\}\right]. \qquad (A7)$$

The improper integral in (A7) is calculated by expanding as a series the term in square brackets:

$$\sum_{j=1}^{\infty}\frac{(-1)^{j+1}}{j!}\left(\frac{2QD\cos\varphi\cos\psi}{\sqrt{2\pi}\eta}\right)^j \times\int_{-\infty}^{\infty}\exp\left[-\left(\frac{2}{\alpha_e^2}+\frac{j}{2\eta^2}\right)\Delta^2\right]\mathrm{d}\Delta$$
$$= \sum_{j=1}^{\infty}\frac{(-1)^{j+1}}{j!}\frac{2QD\cos\varphi\cos\psi}{\sqrt{2\pi}\eta}\cdot\frac{\eta\sqrt{2\pi}}{\sqrt{j+\frac{4\eta^2}{\alpha_e^2}}}. \qquad (A8)$$

Introducing the notation defined in the footnote to Table 1 we obtain (25). In order to derive the expression for the secondary extinction coefficient we calculate the integrated reflectivity without taking into account the secondary extinction:

$$I_{\mathrm{id}}^1(\varphi,\psi) = I_0(0)rD\cos\varphi\cos\psi\exp(-\mu D\cos\varphi\cos\psi),$$

$$P_{\mathrm{id}}(\theta,\Delta) \equiv \frac{P_{\mathrm{id}}^1}{P_0(0)} = \frac{4}{\pi}rD\int_0^{\pi/2}\int_0^{\pi/2}\cos^3\varphi\cos^2\psi \times\exp(-\mu D\cos\varphi\cos\psi)\mathrm{d}\varphi\mathrm{d}\psi,$$

$$R_{\mathrm{id}}^\theta = \frac{4}{\pi}\int_0^{\pi/2}\int_0^{\pi/2}\mathrm{d}\varphi\mathrm{d}\psi\cos^3\varphi\cos^2\psi \times\exp(-\mu D\cos\varphi\cos\psi) \times\int_{-\infty}^{\infty}\frac{QD}{\sqrt{2\pi}\eta}\exp\left[-\left(\frac{1}{2\eta^2}+\frac{2}{\alpha_e^2}\right)\Delta^2\right]\mathrm{d}\Delta$$
$$= \frac{4}{\pi}\sqrt{2\pi}\frac{AC}{\sqrt{B}}\int_0^{\pi/2}\int_0^{\pi/2}\cos^3\varphi\cos^2\psi \times\exp(-C\cos\varphi\cos\psi)\mathrm{d}\varphi\mathrm{d}\psi. \qquad (A9)$$

By dividing (25) by (A9) we obtain (32).

References

ABOV, YU. G. (1960). *Prib. Tekh. Exp.* **2**, 3–12.

BACON, G. E. & LOWDE, R. D. (1948). *Acta Cryst.* **1**, 303–314.

CAGLIOTI, G. & RICCI, F. P. (1962). *Nucl. Instrum. Meth.* **40**, 155–163.

COOPER, M. J. & ROUSE, K. D. (1970). *Acta Cryst.* A**26**, 214–223.

COOPER, M. J., ROUSE, K. D. & FUESS, H. (1973). *Acta Cryst.* A**29**, 49–56.

DIETRICH, O. W. & ALS-NIELSEN, J. (1965). *Acta Cryst.* **18**, 184–188.

DORNER, B. (1971). *J. Appl. Cryst.* **4**, 185–190.

DYMOND, R. R. & BROCKHOUSE, B. N. (1970). *Instrumentation for Neutron Inelastic Scattering Research*, pp. 105–112. Vienna: IAEA.

HAMILTON, W. C. (1957). *Acta Cryst.* **10**, 629–634.

HAMILTON, W. C. (1963). *Acta Cryst.* **16**, 609–611.

JAMES, R. W. (1950). *The Optical Principles of the Diffraction of X-Rays*. London: Bell.

KUNITOMI, N., SAKAMOTO, M., HAMAGUCHI, Y. & BETSUYAKU, H. (1964). *J. Phys. Soc. Japan*, **19**, 2280–2285.

MOON, R. M. & SHULL, C. G. (1964). *Acta Cryst.* **17**, 805–817.

NOSIK, YU. M. (1966). *Zh. Strukt. Khim.* **7**, 916–918.

POPOVICI, M. & GELBERG, D. (1966). *Nucl. Instrum. Meth.* **40**, 77–83.

POPOVICI, M., GHEORGHIU, Z. & GELBERG, D. (1968). Report FN-34, Inst. Fiz. At., Rumania.

RISTE, T. & OTNES, K. (1969). *Nucl. Instrum. Meth.* **75**, 197–202.

SAILOR, V. L., FOOTE, H. L. JR, LANDON, H. H. & WOOD, R. E. (1956). *Rev. Sci. Instrum.* **27**, 26–34.

ZACHARIASEN, W. H. (1945). *Theory of X-Ray Diffraction in Crystals*. New York: John Wiley.

ZACHARIASEN, W. H. (1967). *Acta Cryst.* **23**, 558–564.